NOTICE CONCERNING COPYRIGHT RESTRICTIONS

This document may contain copyrighted materials. These materials have been made available for use in research, teaching, and private study, but may not be used for any commercial purpose. Users may not otherwise copy, reproduce, retransmit, distribute, publish, commercially exploit or otherwise transfer any material.

The copyright law of the United States (Title 17, United States Code) governs the making of photocopies or other reproductions of copyrighted material.

Under certain conditions specified in the law, libraries and archives are authorized to furnish a photocopy or other reproduction. One of these specific conditions is that the photocopy or reproduction is not to be "used for any purpose other than private study, scholarship, or research." If a user makes a request for, or later uses, a photocopy or reproduction for purposes in excess of "fair use," that user may be liable for copyright infringement.

This institution reserves the right to refuse to accept a copying order if, in its judgment, fulfillment of the order would involve violation of copyright law.

Temporal Velocity Variations beneath the Coso Geothermal Field Observed using Seismic Double Difference Tomography of Compressional and Shear Wave Arrival Times

Tim Seher[1], Haijiang Zhang[1], Mike Fehler[1], Haiying Yu[1,2], Veronika Soukhovitskaya[3], Michael Commer[3], and Gregory Newman[3]

[1]Massachussetts Institute of Technology, Cambridge MA
[2]Shanghai Seismology Bureau, China
[3]Lawrence Berkeley National Laboratory, Berkeley CA

Keywords

Coso, geothermal, microearthquake, double difference tomography, Poisson's ratio, time lapse monitoring, joint inversion

ABSTRACT

Microseismic imaging can be an important tool for characterizing geothermal reservoirs. Since microseismic sources occur more or less continuously both due to the operations of a geothermal field and the naturally occurring background seismicity, passive seismic monitoring is well suited to quantify the temporal variations in the vicinity of a geothermal field. We use microseismic data recorded between 1996 and 2008 to determine the temporally varying seismic velocity of the Coso geothermal field.

In this study we will apply the double difference tomography method to simultaneously locate a suite of microseismic events and determine the compressional and shear wave velocity as well as their ratio. In a first step, we apply traveltime tomography based on the observed microearthquake catalog for every single year between 1996 and 2008 to obtain a first model for the subsurface velocities. In the next step we will estimate differential traveltimes using a cross-correlation technique. This allows us to apply double-difference tomography to refine our velocity models separately for each year. The double-difference method uses relative arrival times of earthquakes measured at the same station, which allows a more precise determination of the relative locations of earthquakes. In a final step, we plan to analyze temporal deviations from a reference model integrating the whole dataset between 1996 and 2008.

Introduction

The Coso geothermal field is located between the eastern flank of the Sierra Nevada and the western edge of the Basin and Range tectonic province of southeastern California, and lies within the Walker Lane/Eastern California Shear Zone. The tectonics of the Coso field show a transition between the right slip San Andreas fault-plane and the extensional tectonics of the Basin and Range province. The hot springs in the area are primarily associated with oblique faults (Roquemore, 1979). The Coso geothermal field currently produces nearly 300 MW of electricity from 100 wells with production depths ranging from 600 to 3700 meters.

Microseismic measurements are a valuable tool for the characterization of a geothermal field and allow both structural imaging and the identification of fault and fracture systems. In the Coso geothermal field microseismic tomography studies have identified two low velocity zones for both P- and S-waves at the production depth of the geothermal reservoir (Wu and Lees, 1999; Lees and Wu, 2000). These two low velocity zones also show a lower Poisson's ratio and are separated by a band of high Poisson's ratio and high porosity, which is suspected to represent a conduit or a geothermal reservoir (Lees and Wu, 2000). Vlahovic et al. (2003) identify three fracture systems in the Coso geothermal field based on shear wave splitting measurements. Similarly, Lees (1998) used multiplet analysis to demonstrate that fracture density is largest near injection wells and concludes that cracks are activated by fluid-pressure variations.

We have decided to revisit the seismic structure of the Coso geothermal field for two recent developments. First, strong evidence suggest that temporal velocity changes are observable in the Coso geothermal field (Vlahovic et al., 2003; Julian et al., 2008; Julian and Foulger, 2009, 2010). By applying the microseismic double difference technique (Zhang and Thurber, 2003, 2006), we hope to better constrain the subsurface distribution of P- and S-wave velocities. Second, Newman et al. (2008) have recently shown clear correlation between the subsurface resistivities and velocities. However, the model of Newman et al. (2008) suffers from the non-uniqueness of the inverse problem. By closely integrating seismic and magnetotellurics, we hope to improve the quality of both the final resistivity and velocity models.

Recently, a large microseismic dataset from 1996 to 2008 has become available from the Coso geothermal field (Daniel R.H. O'Connell, Bruce Julian & Wei-Chuang Huang, pers. comm.). In this paper we will describe our first steps towards a new microseismic tomography model for the Coso region.

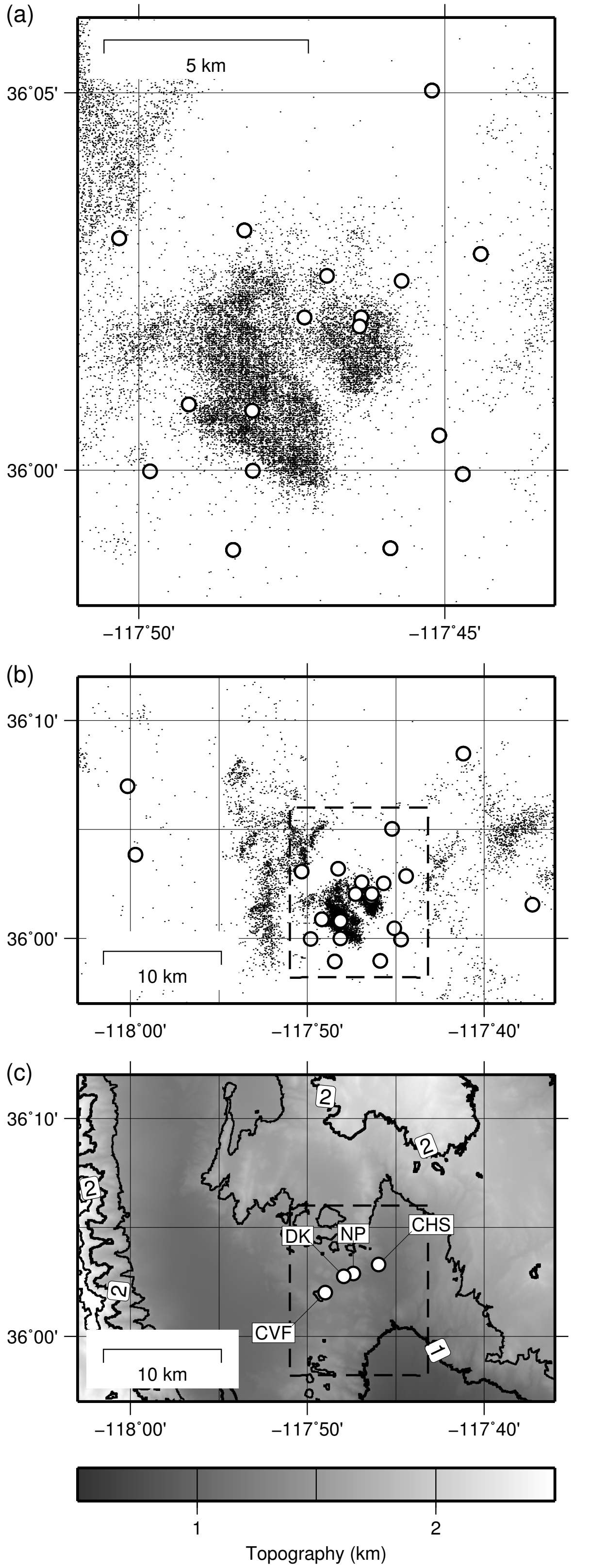

Figure 1. Map of the seismic experiment. (a) Seismicity and seismometers used in our study. (b) Seismicity and seismometers for the whole deployment period. The number of earthquakes has been reduced by a factor 10. (c) Topographic map of the study region. The dashed square marks the region of this study (CVF: Coso volcanic field, DK: Devil's kitchen, NP: Nichol Prospects, CHS: Coso hot springs).

Experiment Geometry and Data Processing

The Coso microseismic experiment registered 107,853 microearthquakes between 1996 and 2008 using 11-16 microseismic stations (figure 1(b)). The seismicity is mostly concentrated to three regions - a linear cluster to the west of the geothermal field, a circular cluster coincident with the geothermal field and a more diffuse cluster to the east of the geothermal region. In our further analysis we focus on the central cluster underneath the geothermal field (figure 1(a)).

The number of microseismic events is large (4,000-13,000 single events per year). We first restrict the events to the region of interest and extract subsets of the data corresponding to one year. Next, we grid the microseismic data using the initial catalog locations. For gridding we divide the subsurface in cells with a side length of 250 m and select those microseismic events with most traveltime picks inside every single grid cell. The gridding reduced the number of microearthquakes to 800-2,300 per year.

To assure self-consistency, assess the data quality and remove outliers from the dataset, we fit a straight line to the traveltime moveout curve. We calculate the straight ray distance between the initial catalog location and the receiver position, remove a linear trend from the traveltime observations and estimate the root mean square traveltime residual σ. Traveltime picks that lie father than $5 \cdot \sigma$ from the best fitting line are removed from the data sets. The number of removed traveltime picks is less than 100 for each year.

The moveout curve allows a first estimation of the subsurface velocities (figure 2). The linear moveout indicates a P-wave velocity of $V_p \approx 5.1$ km/s, a S-wave velocity of $V_s \approx 2.9$ km/s and a Poisson's ratio of ≈ 0.26. These estimates may be biased by the velocity model that was used to estimate the microearthquake catalog locations.

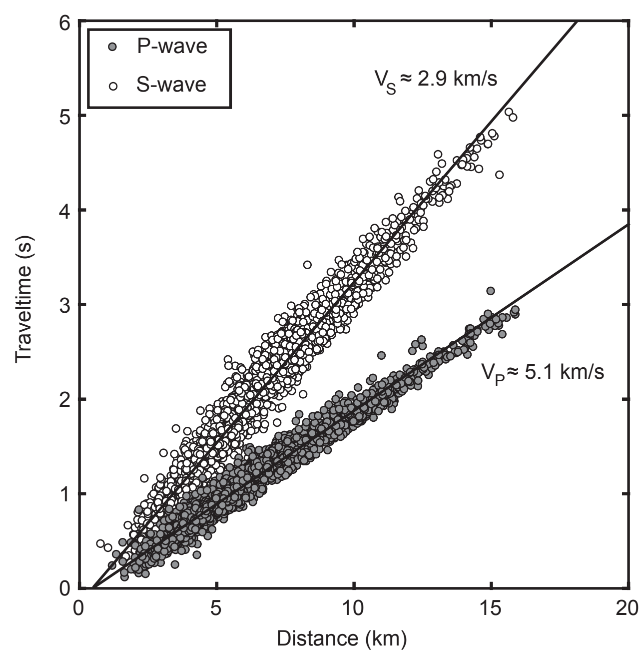

Figure 2. Traveltime moveout for all P- and S-wave observations. The number of picks has been reduced by a factor 10 for plotting. The source-receiver distance has been estimated assuming straight rays and a constant velocity subsurface. The black lines mark the best fitting subsurface velocities.

High quality traveltime picks should be given larger weight in a traveltime tomography algorithm than poor quality picks. The traveltime picks had a traveltime uncertainty assigned by the analysts. The average traveltime uncertainty is 31 ms for the P-wave traveltimes and 54 ms for the S-wave traveltimes. We convert the traveltime uncertainties to a data weight for the inversion. The largest weight is 1 and corresponds to a traveltime uncertainty smaller than 10 ms. The weight decreases linearly until 0.1 for a traveltime uncertainty larger than 90 ms (see figure 3).

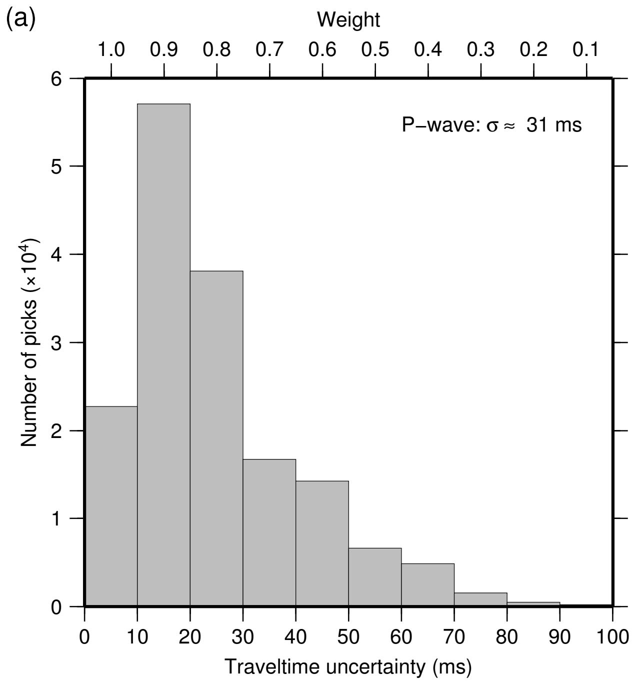

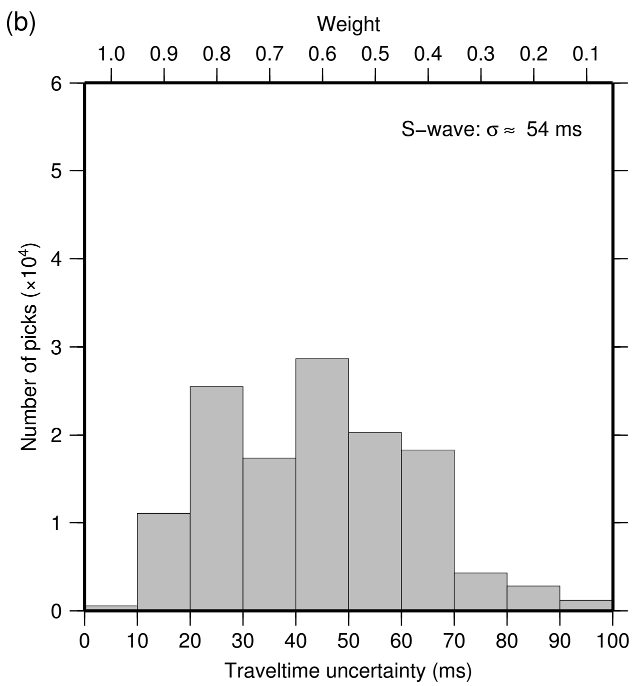

Figure 3. Traveltime uncertainty and number of traveltime picks of both P- and S-wave. The traveltime uncertainty is converted to a weight in the inversion. σ denotes the average traveltime uncertainty for the P- and S-wave picks.

We design the inversion grid by carrying out checkerboard tests. We use a 1D velocity model as background velocity (Julian and Foulger, 2010) and add velocity perturbations with an amplitude of 5%. Next, we estimate synthetic traveltimes assuming the given earthquake catalog locations and add Gaussian noise with a standard deviation of 31 ms and 54 ms for the P- and S-wave, respectively. We then apply double difference tomography algorithm (Zhang and Thurber, 2003, 2006) and compare the recovered velocity perturbations with the known true velocity perturbations. This allows us to assess the lateral resolution and wavelength of anomalies that can be constrained given a distribution of earthquakes. We choose a velocity node spacing of 0.5 km in all spatial dimensions.

Each tomography scheme suffers from the non-uniqueness of the inverse problem. This problem is usually addressed by introducing an additional criterion in the inverse problem. The tomography code (Zhang and Thurber, 2003, 2006) used in this study, applies a flatness constraint to the model update. The value of the flatness with respect to the starting model is constrained by two parameters - the smoothing and the damping λ. In this study we apply an L-curve criterion (cf. Farquharson and Oldenburg, 2004) that allows us to evaluate the trade-off between the model norm, the flatness of the velocity update, and the normalized traveltime misfit.

The L-curve criterion allows us to select optimal combinations of smoothing and damping in a rigorous manner (figure 4). As expected, the model norm increases as the data norm decreases. As the structure in the model increases, the model better explains the data.

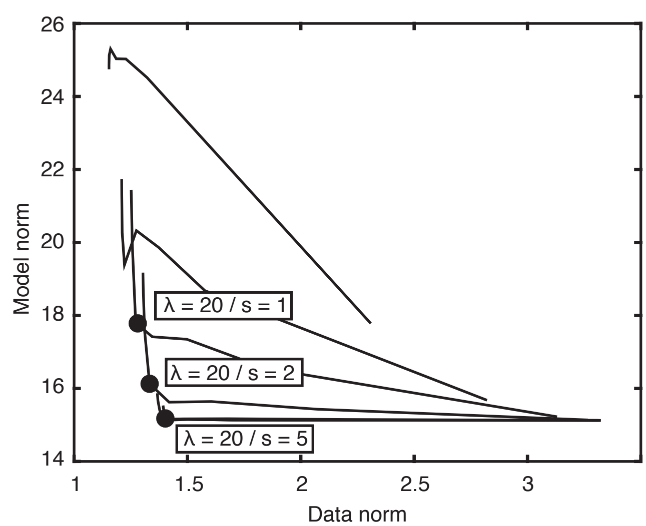

Figure 4. Trade-off curve between data norm and model norm. The data norm is the normalized absolute and differential misfit for P- and S-wave traveltimes. The model norm is the flatness of the velocity anomaly with respect to the starting model. Each line represents one smoothness value s and damping parameters λ between 1 and 1000. The black circles mark the optimal solutions selected from the trade-off curve.

Preliminary Results

We present a preliminary tomography result showing both the P-wave and S-wave anomaly (the perturbation from the starting model). We have used the L-curve criterion described above to select an optimum damping and smoothing (λ=20, s=2).

Our velocity model shows a low velocity zone at a depth of 2-3 km, which corresponds to the zone where geothermal fluids are produced. This low velocity region is cut in half by a region of elevated velocities. Our model is similar to older models (Wu and Lees, 1999; Lees and Wu, 2000) and the low velocity region coincides with a low velocity region in those older models.

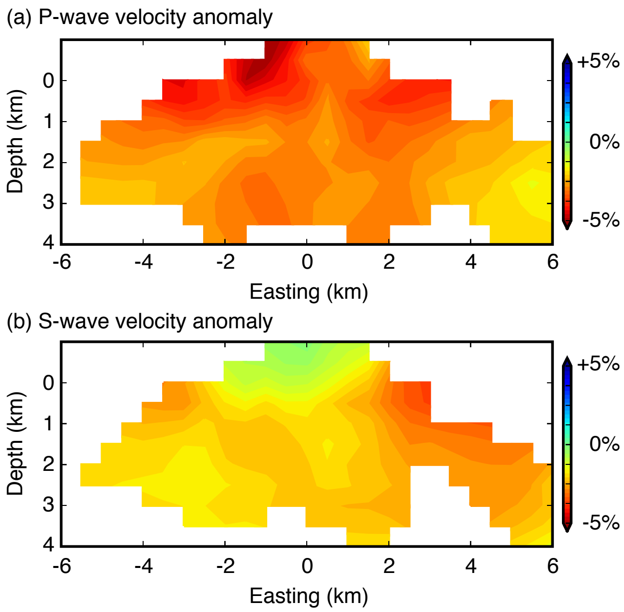

Figure 5. 2D slice through the 3D velocity model running from west to east through the center of the microearthquake cloud shown in figure 1. The slice shows the difference between the final model and the starting model. Model cells not constrained by the seismic data have been masked.

We have found a stable starting model that will be used to further investigate the velocity structure beneath the Coso geothermal field. In particular, the data processing approach described in this study can be applied to analyze temporal velocity changes. To better constrain the velocity models, we are currently estimating relative traveltimes using cross-correlation of both P- and S-wave arrivals.

Acknowledgments

We thank Daniel R.H. O'Connell for collecting the microseismic data from Bruce Julian and Wei-Chuang Huang and merging it into one easily accessible dataset. This study is funded by the Department of Energy under grant DE-AC02-05CH11231. We thank the Geothermal Program Office of the U.S. Navy for collecting and sharing the microseismic data.

References

C.G. Farquharson and D.W. Oldenburg. A comparison of automatic techniques for estimating the regularization parameter in non-linear inverse problems. *Geophys. J. Int.*, 156:411–425, 2004. DOI: 10.1111/j.1365-246X.2004.02190.x.

B.R. Julian and G.R. Foulger. Time-dependent seismic tomography of geothermal systems. In *Thirty-Fourth Workshop on Geothermal Reservoir Engineering*, number SGP-TR-187, Stanford University, Stanford, California, February 2009.

B.R. Julian and G.R. Foulger. Time-dependent seismic tomography. *Geophys. J. Int.*, 182:1327–1338, 2010. ISSN 1365-246X. DOI: 10.1111/j.1365-246X.2010.04668.x.

B.R. Julian, G.R. Foulger, and F.C. Monastero. Time-dependent seismic tomography and its application to the Coso geothermal area, 1996-2006. In *Proceedings, Thirty-Third Workshop on Geothermal Reservoir Engineering*. Stanford University, January 2008.

J.O. Kaven, S. Hickman, and N.C. Davatzes. Micro-seismicity, fault structure, and hydrologic compartmentalization within the coso geothermal field, california, from 1996 until present. In *Eos Trans. AGU*, number H33D-1163, 2010. presented at 2010 Fall Meeting, AGU, San Francisco, Calif., 13-17 Dec.

J.M. Lees. Multiplet analysis at Coso geothermal. *Bulletin of the Seismological Society of America*, 88 (5):1127–1143, 1998. ISSN 0037-1106.

J.M. Lees and H. Wu. Poisson's ratio and porosity at Coso geothermal area, California. *J. Volc. Geoth. Res.*, 95(1-4):157–173, 2000. DOI: 10.1016/S0377-0273(99)00126-2.

G.A. Newman, E. Gasperikova, G.M. Hoversten, and P.E. Wannamaker. 3d magnetotelluric characterization of the COSO Geothermal Field. *Geothermics*, 37:369–399, 2008.

G. Roquemore. Structure, tectonics, and stress field of the Coso Range, Inyo County, California. *J. Geophy. Res.*, 85(B5):2434–2440, 1979.

G. Vlahovic, M. Elkibbi, and JA Rial. Shear-wave splitting and reservoir crack characterization: the coso geothermal field. *J. Volc. Geoth. Res.*, 120(1-2):123–140, 2003. ISSN 0377-0273. DOI: 10.1016/S0377-0273(02)00368-2.

H. Wu and J.M. Lees. Three-dimensional P and S wave velocity structures of the Coso Geothermal Area, California, from microseismic travel time data. *J. Geophy. Res.*, 104(B6):13,217–13,233, 1999.

H. Zhang and C. Thurber. Development and applications of double-difference seismic tomography. *PAGEOPH*, 163(2):373–403, 2006. ISSN 0033-4553. DOI: 10.1007/s00024-005-0021-y.

H. Zhang and C.H. Thurber. Double-difference tomography: the method and its application to the Hayward fault, California. *Bull. Seism. Soc. Am.*, 93(5):1875–1889, 2003. DOI: 10.1785/0120020190.